THE JOURNAL OF BIOLOGICAL CHEMISTRY
Vol. 279, No. 24, Issue of June 11, pp. 25866–25875, 2004
Printed in U.S.A.

HFE and Transferrin Directly Compete for Transferrin Receptor in Solution and at the Cell Surface*

Received for publication, February 10, 2004, and in revised form, March 30, 2004
Published, JBC Papers in Press, March 31, 2004, DOI 10.1074/jbc.M401467200

Anthony M. Giannetti‡ and Pamela J. Björkman§¶

From the ‡Graduate Option in Biochemistry and Molecular Biophysics and the §Division of Biology and Howard Hughes Medical Institute, California Institute of Technology, Pasadena, California 91125

Transferrin receptor (TfR) is a dimeric cell surface protein that binds both the serum iron transport protein transferrin (Fe-Tf) and HFE, the protein mutated in patients with the iron overload disorder hereditary hemochromatosis. HFE and Fe-Tf can bind simultaneously to TfR to form a ternary complex, but HFE binding to TfR lowers the apparent affinity of the Fe-Tf/TfR interaction. This apparent affinity reduction could result from direct competition between HFE and Fe-Tf for their overlapping binding sites on each TfR polypeptide chain, from negative cooperativity, or from a combination of both. To explore the mechanism of the affinity reduction, we constructed a heterodimeric TfR that contains mutations such that one TfR chain binds only HFE and the other binds only Fe-Tf. Binding studies using a heterodimeric form of soluble TfR demonstrate that TfR does not exhibit cooperativity in heterotropic ligand binding, suggesting that some or all of the effects of HFE on iron homeostasis result from competition with Fe-Tf for TfR binding. Experiments using transfected cell lines demonstrate a physiological role for this competition in altering HFE trafficking patterns.

Hereditary hemochromatosis is a prevalent genetic disorder characterized by a defect in a checkpoint of iron homeostasis resulting in the absorption of dietary iron beyond the body's needs. If left untreated, hereditary hemochromatosis results in the deposit of iron primarily in the liver, heart, pancreas, and parathyroid and pituitary glands, leading to pathologies such as arthritis, liver cancer, diabetes, cardiomyopathy, and bronzing of skin (1, 2). Positional cloning revealed that most hereditary hemochromatosis patients carry mutations in the gene coding for a protein called HFE (3). HFE is a membrane protein homologous to class I major histocompatibility complex proteins (3), which present antigenic peptides to T lymphocytes (4). Like class I major histocompatibility complex molecules and most other class I homologs, HFE is a heterodimer in which a membrane-bound heavy chain associates noncovalently with the light chain β_2-microglobulin (3). Most hereditary hemochromatosis patients are homozygous for a mutation that converts residue 260 of the mature HFE protein from cysteine to tyrosine (3), preventing proper folding, β_2-microglobulin association, and cell surface expression and eliminating its effects on cellular iron levels (5–7).

A potential link between HFE and the regulation of iron homeostasis was established by the observation that HFE binds to transferrin receptor 1 (TfR)[1] (8, 9), a homodimeric cell surface glycoprotein that serves as the receptor for iron-loaded transferrin (Fe-Tf) (10). Each chain of the TfR homodimer contains an ~640-residue ectodomain, a glycosylated stalk region, a membrane-spanning segment, and an N-terminal cytoplasmic domain containing a YTRF endosomal sorting signal. This motif serves as a signal for endocytosis and transport back to the cell surface through recycling endosomes (11–13). The extracellular domain of TfR forms a high affinity complex with circulating Fe-Tf and transports it to acidic endosomes. At the low pH of endosomes (pH ≤6.5), TfR assists in the release of iron from Fe-Tf (14, 15). The iron-free form of Tf (apo-Tf) remains bound to TfR inside acidic endosomes and is recycled to the cell surface, where apo-Tf dissociates at the slightly basic pH of the blood (16).

TfR can form a number of complexes with HFE and Fe-Tf (Fig. 1). TfR homodimers bind two Fe-Tf molecules to form Fe-Tf·TfR complexes with 2:1 ligand/receptor stoichiometry (17, 18). Soluble TfR homodimers also bind two HFE molecules to form 2:1 HFE·TfR complexes (19, 20), although 1:1 HFE·TfR complexes can be found in solution using soluble forms of HFE and TfR (18, 20). When all three proteins are present, HFE·TfR·Fe-Tf ternary complexes are observed in solution (18) and in lysates from HFE-transfected HeLa cells (21, 22). Competition (23), mutagenesis (20, 24), time-resolved x-ray footprinting (25), and electron microscopy studies (26) demonstrate that Fe-Tf and HFE compete for overlapping binding sites on each TfR chain; thus, HFE·TfR·Fe-Tf ternary complexes have a 1:1:1 stoichiometry, such that HFE binds to one TfR polypeptide chain and Fe-Tf binds to the other.

Comparison of the crystal structures of TfR alone (27) and a 2:1 HFE·TfR complex (19) reveals that HFE binding induces changes at the TfR dimer interface that are distant from the HFE binding site, suggesting that HFE binding to one polypeptide chain of the TfR dimer can transmit structural changes to the other TfR chain. These changes could influence the binding of Fe-Tf or another HFE to the other side of the TfR dimer. Indeed, in some studies, Fe-Tf binds with a lower apparent affinity to cell surface TfR in the presence of membrane-bound or soluble HFE (8, 21), and an affinity reduction is also ob-

* This work was supported by the Howard Hughes Medical Institute, by National Institutes of Health Grant 1 R01 DK60770 (to P. J. B.), and by National Research Service Award 5T32-GM-7616 (to A. M. G). The costs of publication of this article were defrayed in part by the payment of page charges. This article must therefore be hereby marked "*advertisement*" in accordance with 18 U.S.C. Section 1734 solely to indicate this fact.

¶ To whom correspondence should be addressed: Division of Biology California Institute of Technology, 1200 E. California Blvd., MC 114-96, Pasadena, CA 91125. Tel.: 626-395-8350; Fax: 626-792-3683; E-mail: bjorkman@caltech.edu.

[1] The abbreviations used are: TfR, transferrin receptor; Tf, transferrin; Fe-Tf, iron loaded transferrin; hdTfR, heterodimeric form of soluble TfR; AUC, analytical ultracentrifugation; SPR, surface plasmon resonance; wtTfR, wild type TfR; GFP, green fluorescence protein; NTA, nitrilotriacetic acid; PIPES, 1,4-piperazinediethanesulfonic acid; EGFP, enhanced green fluorescent protein.

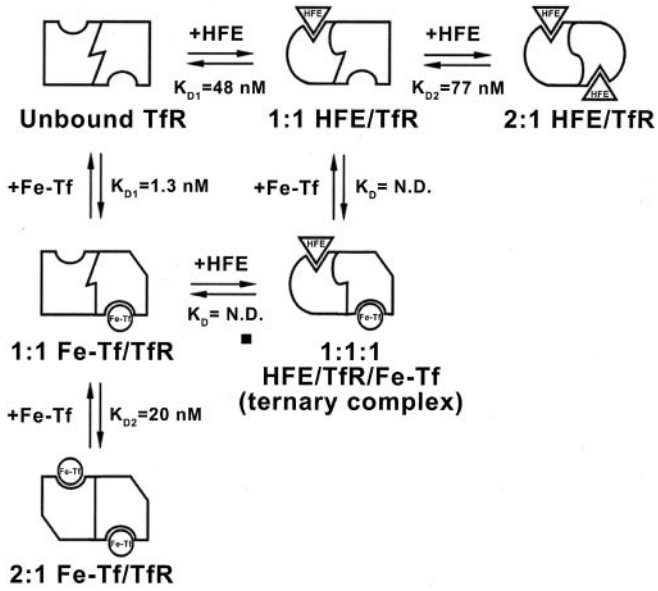

FIG. 1. **Equilibrium relationships for complexes formed by HFE, Fe-Tf, and TfR.** Statistically corrected equilibrium binding constants are shown for binary binding reactions (Table I). *N.D.*, K_D values determined for hdTfR but not wtTfR.

served when Fe-Tf binds to soluble TfR in the presence of soluble HFE (23). The apparent affinity reduction could result from competition between Fe-Tf and HFE for binding to TfR, from negative cooperativity due to structural changes in the unbound TfR chain that are imparted by HFE binding to the other chain, or from a combination of both phenomena.

Investigation of the mechanism by which HFE influences the binding of Fe-Tf to TfR is complicated, because complexes in addition to the HFE·TfR·Fe-Tf ternary complex form in an equilibrium mixture of the three proteins (Fig. 1). Thus, previous quantitative binding studies have derived equilibrium dissociation constants (K_D values) only for binary HFE·TfR and Fe-Tf·TfR complexes (18, 20, 24, 28). Using Fe-Tf, a soluble serum protein, and recombinant soluble forms of HFE and TfR, we previously measured equilibrium dissociation constants (K_D values) for the first (K_{D1}) and second (K_{D2}) binding events to homodimeric TfR, demonstrating that HFE binds with lower affinity to TfR than does Fe-Tf (18, 20, 24) (Fig. 1). In this study, we examine how binding of HFE or Fe-Tf to one side of the TfR dimer affects binding to the other chain in the absence of the competing binary complexes, using a heterodimeric form of soluble TfR (hdTfR) in which one chain can bind HFE and not Fe-Tf and the other chain can bind Fe-Tf but not HFE. Using analytical ultracentrifugation (AUC) and surface plasmon resonance (SPR) binding assays, we verified that hdTfR binds one HFE and one Fe-Tf. We then measured the affinity of the free TfR chain for Fe-Tf (or HFE) when HFE (or Fe-Tf) is bound to the other chain. We found no affinity reduction for Fe-Tf or HFE binding to hdTfR in the presence of saturating amounts of the other ligand, suggesting that direct competition, rather than negative cooperativity, is responsible for the apparent affinity reduction in Fe-Tf binding to cell surface and soluble TfR in the presence of HFE.

Having determined that HFE lowers the apparent affinity for Fe-Tf by directly competing for TfR binding sites rather than through an allosteric mechanism, we evaluated the effects of this competition at physiological concentrations of Fe-Tf using HFE and TfR expressed in transfected cells. We first demonstrate that a green fluorescent protein (GFP)-tagged form of HFE is dependent on its association with TfR for transport to Tf-positive endosomal compartments. We then show that the addition of Fe-Tf to the cellular media induces a redistribution of HFE within the cells, suggesting that fluctuations in serum Fe-Tf concentration can significantly alter the stoichiometric ratios of the possible TfR complexes and free proteins at the cell surface. These results are discussed in terms of the role of HFE in the control of cellular iron homeostasis.

EXPERIMENTAL PROCEDURES

Production of Wild-type Proteins—Soluble wtTfR was produced in a lytic baculovirus/insect cell expression system as previously described (18). Briefly, we used a modified version of the pAcGP67A expression vector (Pharmingen) that codes for the gp67 hydrophobic leader sequence followed by a His_6 tag, factor Xa cleavage site, and residues 121–760 of human TfR. Soluble human HFE/β2-microglobulin heterodimers were expressed in Chinese hamster ovary cells and purified as previously described (18). Human Fe-Tf was prepared from apo-Tf (Sigma) by incubation with bicarbonate and excess ferric ammonium sulfate.

Expression of hdTfR and Homodimeric TfR Mutants—Mutations (L619A/Y643A for the Fe-Tf-binding TfR chain and Y123S/G647A/R651A for the HFE-binding TfR chain) were introduced into the expression vector encoding human wtTfR (wild-type TfR) using the QuikChange™ protocol (Stratagene). Constructs were verified by sequencing of the protein-coding region. His-tagged mutant TfR homodimers were expressed in baculovirus-infected insect cells and purified as described above. For production of hdTfR, the L619A/Y643-TfR construct was mutagenized further to exchange the His_6 tag for the StrepTag II affinity tag (WSHPQEK) (29), a sequence designed to bind to streptactin, a modified form of streptavidin (30). PCR was used to introduce restriction sites and a ribosomal binding sequence (CCTATAAAT) immediately upstream of the start codon and to amplify the coding regions of the L619A/Y643A-TfR and Y123S/G647A/R651A-TfR constructs. The mutant TfR sequences were ligated into the pFastBacDUAL (Invitrogen) dicistronic baculovirus expression vector. The gene encoding Y123S/G647A/R651A-TfR was ligated 3′ to the p10 promoter site using SphI and XhoI restriction sites, and the gene encoding L619A/Y643A-TfR was ligated downstream of the polyhedron promoter using BssHII and NotI restriction sites. Recombinant viruses were generated by co-transfection of a transfer vector with linearized viral DNA (Baculogold, Pharmingen) for TfR homodimers or by use of the Bac-to-Bac® system (Invitrogen) for hdTfR.

Purification of hdTfR—Separation of the three species of TfR produced by insect cells expressing both mutant TfR chains (HFE-binding homodimers, Fe-Tf-binding homodimers, and hdTfR) was achieved using sequential affinity chromatography steps. Infected insect cell supernatants containing the secreted TfR species were concentrated and exchanged into 50 mM Tris, pH 7.4, 300 mM NaCl, 10% glycerol, and 15 mM imidazole. Supernatants were passed over a Ni^{2+}-NTA Superflow agarose column (Qiagen), and the two His-tagged species (Fe-Tf-binding homodimers and hdTfR) were eluted from the column with 250 mM imidazole. The eluted peak was loaded onto a 15-ml streptactin-Sepharose column (Sigma-Genosys). After washing with a buffer containing 50 mM PIPES, pH 7.4, and 150 mM NaCl, the column was eluted by the addition of the same buffer with 3 mM desthiobiotin to obtain hdTfR. The column was regenerated by the addition of 1 mM 4-hydroxyazobenzene-2-carboxylic acid, which was removed by washing the resin according to the manufacturer's instructions. Due to low levels of nonspecific binding of the different TfRs to the Ni^{2+}-NTA and streptactin resins, the columns were washed extensively after loading (>20 column volumes for Ni^{2+}-NTA superflow and >5 column volumes for streptactin superflow), which eliminated homodimer carry-through. The purity of hdTfR was monitored throughout the purification process by reverse-phase fast protein liquid chromatography using a Resource Phe column (Amersham Biosciences). $(NH_4)_2SO_4$ was added to protein samples to a concentration of 850 mM prior to loading on the column, and proteins were eluted by a gradient from 850 to 0 mM $(NH_4)_2SO_4$ over 20 column volumes. The two contaminating homodimers resolve into well separated peaks with the hdTfR appearing as a peak between them, as verified by Western blotting using the anti-penta-His antibody (Qiagen) and alkaline phosphatase-conjugated streptactin (IBA) (data not shown). After elimination of detectable contaminating TfR homodimers, hdTfR samples were passed over a Superdex-200 column (Amersham Biosciences) to remove aggregates and exchanged into 50 mM PIPES, pH 7.4, 150 mM NaCl, and 0.05% NaN_3.

Circular Dichroism—CD spectra and thermal denaturation profiles were obtained using an Aviv 62A DS spectrometer with a thermoelec-

tric cell holder and cuvette with a 1-mm path length. Measurements were recorded using samples containing 5 μM TfR protein in 20 mM PIPES, pH 7.4, and 80 mM NaCl. Wavelength scans were collected from 200 to 250 nm in 1-nm increments. For thermal melts, the CD signal at 220 nm was recorded every 1 °C from 4 to 99 °C with an equilibration time of 2 min and an averaging time of 1 min.

Biosensor Analyses—All biosensor experiments were carried out using a BIACORE 2000 instrument (Amersham Biosciences). Interactions between a protein immobilized on the sensor chip (the "ligand") and a protein injected over the sensor surface (the "analyte") are monitored in real time as a change in surface plasmon resonance as measured in resonance units (31, 32). Sensor chips were prepared using standard primary amine coupling chemistry to attach 2000–4000 resonance units of the anti-penta-His antibody (Qiagen) (BIACORE manual), which was used to capture wtTfR and homodimeric TfR mutants (two His tags) directly from insect cell supernatants as described (24). hdTfR was covalently immobilized using primary amine chemistry (BIACORE manual). In each experiment, one of the four flow cells of a CM5 biosensor chip (Amersham Biosciences) was mock-coupled with antibody but no TfR for use as a reference cell. Binding data were collected as previously described (24).

Kinetic sensorgram data were pre-processed using Scrubber (BioLogic Software Pty. Ltd.; available on the World Wide Web at www.biologic.com.au), and kinetic constants were determined by simultaneously fitting the association and dissociation phases of all curves using the Clamp99 program (33) to either a 1:1 model or a bivalent ligand (2:1) model. The 1:1 model describes a simple bimolecular interaction and yields single association (k_{on}) and dissociation (k_{off}) values. The bivalent ligand model describes the sequential binding of two analyte molecules to a homodimeric ligand. This two-step process yields apparent association ($k_{1on,app}$, $k_{2on,app}$) and dissociation ($k_{1off,app}$, $k_{2off,app}$) values for each of the two reactions as follows,

$$A + TfR \leftrightarrow A{:}TfR \text{ (rate constants: } k_{1on,\,app} \text{ and } k_{1off,\,app})$$

REACTION 1

$$K_{D1,\,app} = k_{1off,\,app}/k_{1on,\,app} \quad \text{(Eq. 1)}$$

$$A + A{:}TfR \leftrightarrow A_2{:}TfR \text{ (rate constants: } k_{2on,app} \text{ and } k_{2off,app})$$

REACTION 2

$$K_{D2,app} = k_{1off,app}/k_{1on,app} \quad \text{(Eq. 2)}$$

where A represents either HFE or Fe-Tf. The apparent rate constants can be converted to intrinsic rate constants (k_{1on}, k_{2on}, k_{1off}, and k_{2off}) by applying statistical factors to account for the two potential binding sites on a homodimeric TfR to which the first analyte molecule can bind and the two sites on the fully bound TfR from which the first dissociation event can occur. Thus, the intrinsic rate constants are related to the apparent rate constants such that $k_{1on} = k_{1on,app}/2$ and $k_{2off} = k_{2off,app}/2$ for independent binding sites. Apparent and intrinsic rates and their relative dissociation constants are reported in Table I to facilitate comparison with our previous studies (20, 24).

To evaluate cooperativity in ligand binding, both hdTfR and wtTfR were chemically coupled because of the requirement for base line stability over the period of 2 days. A concentration series of HFE or Fe-Tf was injected to determine binding affinities in a buffer of 50 mM PIPES, pH 7.4, 150 mM NaCl, 0.005% (v/v) surfactant P-20. The concentration series was then repeated with the analyte diluted into a buffer to which 50 μM Fe-Tf or 10 μM HFE had been added. Equilibrium binding data were collected and processed as previously described (24).

Analytical Ultracentrifugation—Sedimentation velocity experiments were performed at 25 °C in a Beckman XL-I Ultima analytical ultracentrifuge using absorbance optics. Protein concentrations were determined spectrophotometrically at 280 nm using extinction coefficients of 187,199 M^{-1} cm^{-1} (wtTfR dimer), 190,230 M^{-1} cm^{-1} (hdTfR), 89,120 M^{-1} cm^{-1} (HFE/β_2-microglobulin), and 111,399 M^{-1} cm^{-1} (Fe-Tf). The concentrations of wtTfR and hdTfR were fixed at 2.5 μM for all experiments. HFE and Fe-Tf were added at the indicated relative molar ratios to TfR (see Fig. 4). Samples were brought to a final volume of 350–420 μl and loaded into two-sector, charcoal-filled epon centerpieces with quartz windows and placed in a four-hole An-60 titanium rotor. Samples were spun at 32,000, 34,000, or 36,000 rpm. Individual scans were collected at 250 or 280 nm with a step size of 0.005 cm until samples reached the bottom of the cell. Data were fit with the program SEDFIT 8.7 (34) using the $c(s)$ analysis routine, which calculates the differential distribution of sedimentation coefficients with an explicit treatment of sample diffusion. The reported apparent sedimentation coefficients (s^*) values are not corrected to standard conditions because of difficulties obtaining partial specific volumes of the glycosylated HFE, TfR, and Fe-Tf proteins.

Generation of HFE-GFP-expressing TRVb and TRVb-1 Cells—PCR was used to amplify the enhanced green fluorescent protein (EGFP) gene in the pEGFP-1 vector (Clontech) to remove the start codon and introduce a 5′ in-frame XhoI site and 3′ HindIII site. The modified gene was subcloned into pBluescript II SK$^-$ (Stratagene). PCR was used to introduce a 5′ Asp718 site and an in-frame 3′ XhoI site at the 3′-end of the human *HFE* gene, which was then introduced into the EGFP Bluescript vector. The resulting open reading frame encoded the entire HFE amino acid sequence, a leucine-glutamate linker region, and EGFP without its N-terminal methionine. The HFE-EGFP chimeric gene was subcloned after sequencing into the mammalian cell expression vector pCB6-HindIII (gift of Ira Mellman, Yale University), which carries a neomycin resistance gene for G418 selection (35).

TRVb and TRVb-1 cell lines were a generous gift from Dr. Timothy McGraw (Cornell University) (36). Both cell lines were maintained in Ham's F-12 medium (Sigma) supplemented with 10% fetal bovine serum, 2 mM glutamine, 12 mM glucose, and 400 μg/ml G418 (TRVb-1 and transfected cells only). Cells were grown to >90% confluence prior to transfections, which were performed using the HFE-GFP expression vector, a human β_2-microglobulin expression vector (18), and the LipofectAMINE 2000 kit (Invitrogen) according to the manufacturer's directions. Clones exhibiting green cell surface fluorescence were isolated using limiting dilution 2 days after transfection. Cells were sorted for GFP fluorescence using a Coulter Elite flow cytometer (Beckman Coulter Inc.) to isolate cells with a medium level of GFP fluorescence.

Confocal Microscopy—Cells were dissociated using trypsin-free dissociation buffer (Invitrogen), seeded onto glass coverslips in 6-well plates, and grown to confluence. For redistribution experiments, the culture medium was removed and replaced with medium containing varying concentrations of human Fe-Tf (Sigma) or chicken iron-loaded ovo-transferrin (Sigma), and cells were incubated at 37 °C in a 5% CO_2 incubator for 1 h. The culture dishes were then placed on ice and washed three times with ice-cold phosphate-buffered saline. Cells were then fixed at 4 °C for 30 min in 4% paraformaldehyde in phosphate-buffered saline, washed in cold phosphate-buffered saline, and mounted on glass slides using Vecta Shield mounting media (Vector Laboratories, Burlingame, CA). For Tf colocalization experiments, cells were incubated for 1 h at 37 °C with 15 μg/ml Alexa-546-conjugated human Fe-Tf (Molecular Probes, Inc., Eugene, OR) in growth medium and processed as above.

Cells were imaged on a Zeiss LSM Pascal Inverted confocal microscope using a × 63 oil immersion Apochromat objective (numerical aperture 1.4). GFP was excited by the 488-nm line from an argon/krypton laser, and Alexa-546-labeled human Fe-Tf was imaged using the 543-nm line from a helium/neon laser. Two-color data were collected in multitracking mode to prevent fluorophore cross-talk. Images were collected and processed with a Zeiss LSM image examiner. Reported images are 1-μm sections collected 2–3 μm above the basal side of the cell.

RESULTS

Production of a Heterodimeric Transferrin Receptor—To construct a TfR heterodimer (hdTfR) in which one chain only binds HFE and the other chain only binds Fe-Tf, we first identified mutations in human TfR homodimers that eliminate binding of one TfR ligand while having a minimal effect on binding of the other ligand. The choice of residues to substitute was complicated by the fact that the HFE and Fe-Tf binding sites overlap on the surface of TfR; thus, many residue substitutions that reduce binding of one ligand also reduce binding of the other (20, 24). We therefore sought to identify mutations that keep the K_D value for binding the desired ligand within the micromolar to nanomolar range while reducing the affinity for binding to the undesired ligand to a >10 μM or higher K_D. Our choice of TfR substitutions was based on results from previous measurements of the affinities of mutant TfRs for Fe-Tf and HFE (24). To create a TfR chain that binds Fe-Tf but not HFE, we combined substitutions L619A and Y643A, each of which eliminates detectable HFE binding but has a more limited effect on Fe-Tf binding (13- and 27.5-fold affinity reductions,

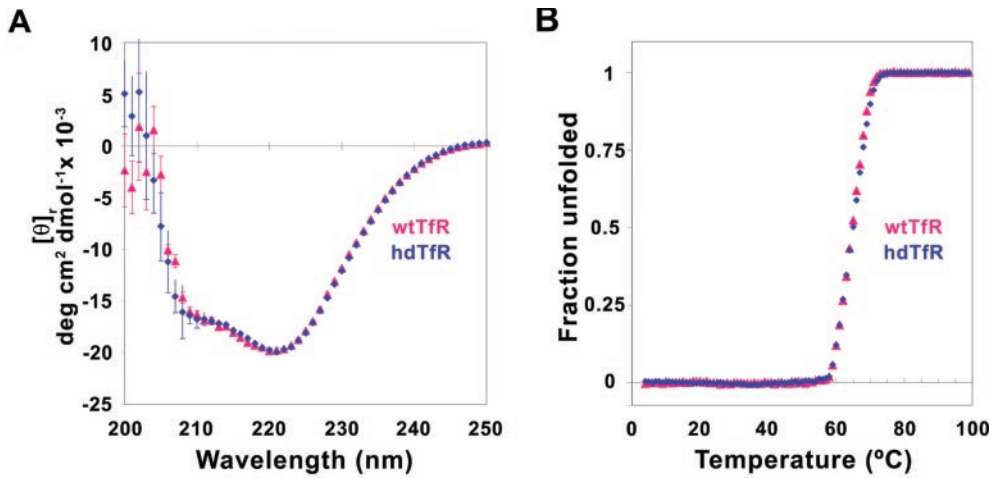

FIG. 2. **Circular dichroism spectra and thermal denaturation profiles of wtTfR (*pink triangles*) and hdTfR (*blue diamonds*).** *A*, far-UV CD spectra of wtTfR and hdTfR. The measured CD signal is given as $[\theta]_r$, the molar ellipticity per residue. Data points represent the average and standard deviation of three (wtTfR) or five (hdTfR) replicate scans. *B*, comparison of thermal denaturation profiles for wtTfR and hdTfR. The CD signal at 220 nm was monitored as a function of increasing temperature and plotted as fraction unfolded after normalization. The transition midpoints derived from a plot of $d[\theta]_r/dT$ *versus* T are 64.8 °C for wtTfR and 65.0 °C for hdTfR.

respectively) (20, 24). To create a TfR mutant that binds HFE but not Fe-Tf, we combined three substitutions: Y123S, G647A, and R651A. Each of these mutations has a significant effect on Fe-Tf binding (8.3-, 222-, and >2,800-fold affinity reductions, respectively) (20, 24). Of these, only one substitution (G647A) exhibits any measurable effect on HFE binding (2.6-fold affinity reduction) (20, 24).

An hdTfR composed of one non-HFE binding and one non-Fe-Tf binding chain was produced by co-expression of the two mutant TfR chains in baculovirus-infected cells. To aid in purification, the Fe-Tf-binding TfR chain contained an N-terminal StrepTagII sequence (29), and the HFE-binding TfR chain contained a His_6 tag. Expression in infected insect cells yields three TfR dimers: HFE- but not Fe-Tf-binding homodimers, Fe-Tf- but not HFE-binding homodimers, and hdTfR. Sequential passage of baculovirus supernatants over a Ni^{2+}-NTA column and a streptactin (30) column resulted in separation of hdTfR from the mutant TfR homodimers and from other proteins in the media. hdTfR appeared to be a stable species, since we found no evidence of homodimers or monomers in hdTfR samples stored for up to 2 months (data not shown). The far UV CD spectra (Fig. 2*A*) and thermal denaturation (Fig. 2*B*) profiles of wtTfR and hdTfR showed no significant differences, demonstrating that the mutations introduced into the hdTfR do not adversely affect its folding or stability.

Binding Affinities of HFE and Fe-Tf to hdTfR and Homodimeric TfR Mutants—Affinities of wtTfR and the mutant TfRs were measured in an SPR-based assay for binding to a soluble form of human HFE or to human Fe-Tf at pH 7.4 (18, 20, 24). Doubly His-tagged wtTfR and homodimeric TfR mutants were captured on biosensor chips using a covalently coupled anti-His tag antibody (20, 24), and the hdTfR was chemically coupled using primary amine chemistry (see "Experimental Procedures"). Either HFE or Fe-Tf was then injected over the TfR-coupled sensor chip. Binding data were fit to a bivalent ligand model in which equilibrium dissociation constants (K_{D1} and K_{D2}) are derived for binding to the first and the second binding sites on homodimeric wild-type and mutant TfRs (Table I and Fig. 3) or to a 1:1 binding model in the case of hdTfR. The Y123S/G647A/R651A mutant homodimer does not detectably bind Fe-Tf at any tested concentration (up to 60 μM) (Fig. 3*B*). Its binding affinity for HFE (Fig. 3*A*) was reduced 2.8-fold relative to wtTfR, consistent with the 2.6-fold reduction observed for the G647A mutant in our previous studies (20, 24). The slight affinity reduction resulted from an increased off-rate compared with wtTfR (Table I). The L169A/Y643A mutant homodimer exhibited no detectable binding to HFE (at concentrations up to 20 μM) (Fig. 3*C*), and its affinity for Fe-Tf was reduced ~500-fold (Fig. 3*D*), again due to an increased off-rate (Table I). We previously demonstrated that the loss in free energy for binding Fe-Tf for the two single mutants that compose the L619A/Y643A mutant is 1.5 kcal/mol (L619A) and 2.0 kcal/mol (Y643A), predicting a $\Delta\Delta G$ value of 3.5 kcal/mol at 25 °C for the double mutant if the two substitutions act independently (24). Consistent with this prediction, the observed 502-fold loss of binding affinity for the L169A/Y643A mutant (Table I) corresponded to a $\Delta\Delta G$ of 3.7 kcal/mol at 25 °C.

The binding data for the mutant TfR homodimers were then compared with binding data for hdTfR. The better fit of the 1:1 binding model to binding reactions involving hdTfR (Fig. 3, *G* and *H*) compared with wtTfR (Fig. 3, *E* and *F*, 1:1 model and residuals) suggests that hdTfR forms 1:1 complexes with Fe-Tf and with HFE. Analysis of the differences in derived binding constants is complicated by the use of different binding models for hdTfR or homodimeric TfRs: a 1:1 binding model for the hdTfR yields a single value for the K_D, whereas the bivalent ligand model describing binding to the homodimeric TfRs yields K_D values describing the first and second binding events (see "Experimental Procedures"). The derived K_D values for the HFE-binding and Fe-Tf-binding chains of the hdTfR are within 3-fold of statistically corrected K_{D1} values for their respective homodimeric mutants (Table I), suggesting that hdTfR does not have significantly altered binding affinities relative to the homodimeric mutants from which it was derived.

Determination of Ligand-binding Stoichiometries of wtTfR and hdTfR—To further compare the ligand-binding properties of hdTfR and wtTfR, we used sedimentation velocity AUC. Velocity AUC data were analyzed using the $c(s)$ size distribution method in the program SEDFIT 8.7 (34). This method fits the data numerically to the Lamm equation and yields a differential distribution of s^* values while explicitly correcting for diffusion of the sedimenting species. The output is displayed as a continuous distribution of s^* values *versus* the $c(s^*)$ function describing the distribution of molecular masses in solution.

We first determined the sedimentation properties of binary HFE·TfR and Fe-Tf·TfR complexes. Each of the individual proteins migrates as a single sharp peak when spun alone (Fig. 4, *dashed black lines labeled HFE*, *Fe-Tf*, *wtTfR*, or *hdTfR*). Fig.

TABLE I
HFE and Fe-Tf binding to TfR constructs at 25 °C

Kinetic and equilibrium constants derived from fitting of the surface plasmon resonance data shown in Fig. 3. Numbers in parentheses are corrected for statistical factors (see "Experimental Procedures"). NB, no binding detected at concentrations of injected analyte up to 80 μM Fe-Tf or 20 μM HFE.

Ligand (immobilized protein)	Analyte (injected protein)	k_{on1}	k_{off1}	k_{on2}	$k_{off}2$	K_{D1}	K_{D2}	K_{D1}, K_{D2} (relative to wild type)
		$M^{-1}s^{-1}$	s^{-1}	$M^{-1}s^{-1}$	s^{-1}	nM	nM	
wtTfR	HFE	3.7×10^6 (1.8×10^6)	0.09	2.6×10^6	0.37 (0.20)	24 (48)	154 (77)	
wtTfR	Fe-Tf	1.7×10^6 (8.3×10^5)	1.0×10^{-3}	1.6×10^5	5.8×10^{-3} (3.2×10^{-3})	0.6 (1.3)	40.6 (20.3)	2.8, 2.5
Y123S/G647A/R651A-TfR	HFE	3.6×10^5 (1.8×10^6)	0.25	2.2×10^6	0.82 (0.41)	67 (134)	384 (192)	
Y123S/G647A/R651A-TfR	Fe-Tf					NB	NB	>27,000
L619A/Y643A-TfR	HFE					NB	NB	>800
L619A/Y643A-TfR	Fe-Tf	5.2×10^5 (2.4×10^5)	0.15	1.5×10^5	0.46 (0.23)	314 (627)	2,940 (1,470)	502, 73
hdTfR	HFE	6.8×10^5	0.27			390		8.1
hdTfR	Fe-Tf	1.9×10^5	0.23			1,210		930

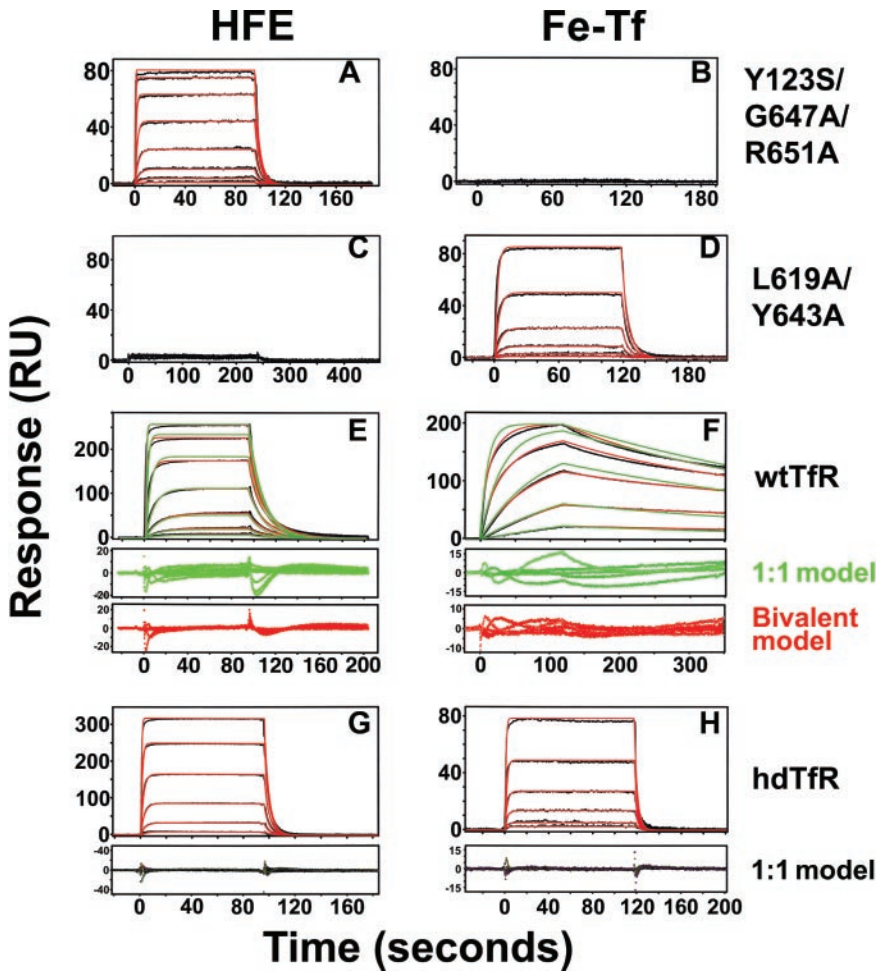

FIG. 3. **SPR analysis of HFE and Fe-Tf binding to TfR proteins.** Experimentally observed response (*black lines*) of HFE or Fe-Tf binding to the indicated TfR molecules is shown with superimposed best fit binding curves (*colored lines*) derived from a bivalent ligand binding model (wtTfR and homodimeric mutant TfRs except where noted) or a 1:1 binding model (hdTfR). Residual plots (difference between the observed and calculated binding data) are shown in *E–H below* the response data. The wtTfR binding data shows fits and residuals for both 1:1 (*green*) and bivalent ligand (*red*) binding models. The highest concentrations in the injection series for each sensorgram are 5 μM (*A*), 60 μM (*B*), 20 μM (*C*), 6 μM (*D*), 2 μM (*E*), 111 nM (*F*), 1.6 μM (*G*), and 10 μM (*H*). Subsequent injections are related by 3-fold dilutions.

4*A* shows the results of mixing HFE and wtTfR in molar ratios of 1:1, 2:1, 4:1, and 6:1, confirming previous findings of both 1:1 and 2:1 HFE/TfR complexes in solution (18, 20), with 2:1 being the terminal stoichiometry as indicated by the presence of excess HFE at the higher mixing ratios. By contrast, mixing excess HFE in the presence of hdTfR resulted in a peak corresponding to a 1:1 HFE·TfR complex, confirming that hdTfR does not readily form 2:1 HFE·TfR complexes (Fig. 4*D*). Analogous experiments were performed to investigate binary interactions of Fe-Tf with wtTfR and hdTfR. Fig. 4*B* shows the results of mixing Fe-Tf and wtTfR at various ratios, confirming previous reports of a 2:1 terminal Fe-Tf/TfR stoichiometry (17, 18). Here we note evidence for formation of a 1:1 Fe-Tf·TfR complex at the 1:1 mixing ratio, which, although predicted to be present in an equilibrium mixture of Fe-Tf and TfR (Fig. 1), has not been previously reported. Mixing Fe-Tf with hdTfR resulted in two connected peaks in the $c(s^*)$ distribution (Fig. 4*E*). The smaller peak represents free hdTfR, and the larger peak is due to the 1:1 Fe-Tf·hdTfR complex. The slightly different position for the 1:1 Fe-Tf·hdTfR peak compared with the position for the 1:1 Fe-Tf·wtTfR peak results from the faster kinetics of complex association and dissociation for hdTfR compared with wtTfR (Table I). We see no evidence of a 2:1 Fe-Tf·hdTfR complex (Fig. 4*E*).

We next used sedimentation velocity AUC to characterize the complexes formed when hdTfR and wtTfR are mixed with both HFE and Fe-Tf. At a mixing ratio of 1:1:1 HFE/wtTfR/Fe-Tf, a broad peak centered at 11.8 S was observed (Fig. 4*C*). The

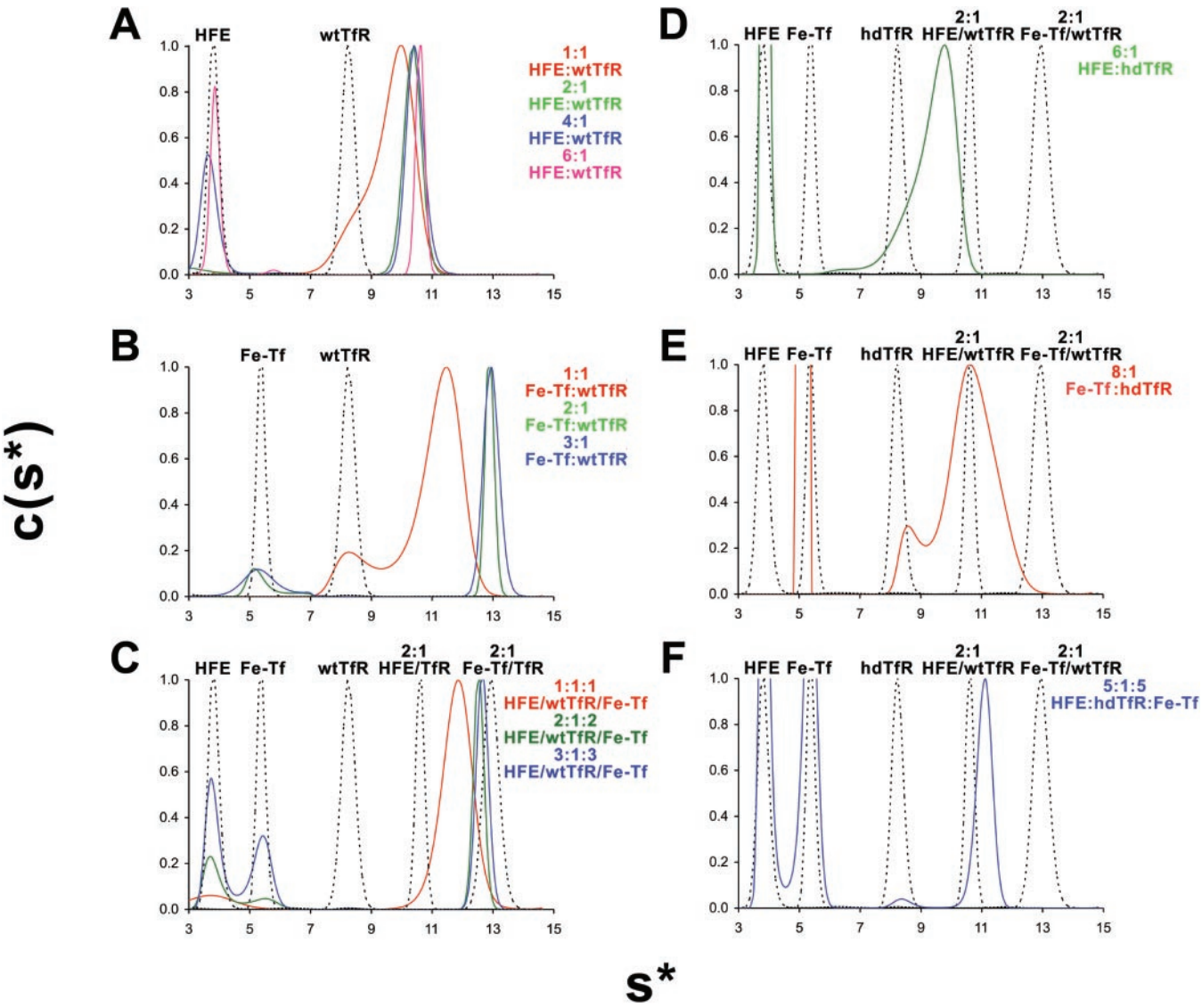

FIG. 4. **Stoichiometries of HFE and Fe-Tf binding to wtTfR and hdTfR from sedimentation velocity ultracentrifugation.** The $c(s^*)$ distribution was determined for each protein alone or in the mixing ratio indicated to the *right* of each *panel*. Reference curves for individual proteins or specific complexes are shown as *dotted black lines*. Peak heights were normalized to the height of the species with the largest s^* value in the distribution.

location of the center of the peak midway between the peaks for the 2:1 HFE·wtTfR and 2:1 Fe-Tf·wtTfR complexes and the fact that the peak spans the positions of the binary complexes are consistent with identification of this peak as a mixture of the 1:1:1 HFE·TfR·Fe-Tf ternary complex with binary 2:1 Fe-Tf·TfR and 2:1 HFE·TfR complexes (Fig. 4*C*, *red curve*). Mixing of the three proteins at higher ligand ratios (2:1:2 and 3:1:3 HFE/TfR/Fe-Tf) resulted in a peak closer to the one observed for 2:1 Fe-Tf/TfR, demonstrating that Fe-Tf effectively competes HFE away from TfR in solution, due to the intrinsically higher TfR binding affinity of Fe-Tf compared with soluble HFE. Mixing of HFE and Fe-Tf with the hdTfR also resulted in a peak between the 2:1 HFE·wtTfR and 2:1 Fe-Tf·wtTfR complexes (Fig. 4*F*). The distribution was more narrow for the ternary complex involving hdTfR, consistent with the expectation that binary complexes with a 2:1 ligand/hdTfR stoichiometry do not form.

Comparison of HFE and Fe-Tf Binding to hdTfR and wtTfR Rules Out Cooperativity in Ligand Binding—Having demonstrated that the engineered hdTfR binds to one HFE and one Fe-Tf to form a ternary complex, we could use the hdTfR to evaluate the potential for heterotropic cooperativity in ligand binding in the absence of the competition observed when using wtTfR. Cooperativity in binding was assessed using an SPR-based binding assay to compare the binding behavior for either HFE or Fe-Tf to hdTfR in the presence and absence of excess Fe-Tf or HFE. If cooperativity is a feature of TfR interactions with HFE or Fe-Tf, then incubation of TfR with saturating amounts of one ligand will perturb the equilibrium binding curve of the second ligand. For these experiments, wtTfR and hdTfR were immobilized on adjacent flow cells of the same sensor chip using primary amine coupling chemistry. We then evaluated the binding of HFE to each TfR in the presence and absence of a saturating concentration of Fe-Tf (50 μM). Binding data were collected using an equilibrium-based approach in which binding reactions reached or closely approached equilibrium. Data for HFE binding to hdTfR in the presence and absence of Fe-Tf (Fig. 5*B*) showed no significant differences, indicating that binding of Fe-Tf to one chain of TfR does not alter the binding properties of the other chain for HFE. Similarly, the binding of Fe-Tf for hdTfR was not altered by the presence of a saturating amount of HFE (10 μM) (Fig. 5*D*). By contrast, when the same binding experiments were performed with wtTfR, we observed competition between HFE and Fe-Tf for binding to TfR. When HFE was injected in the presence of

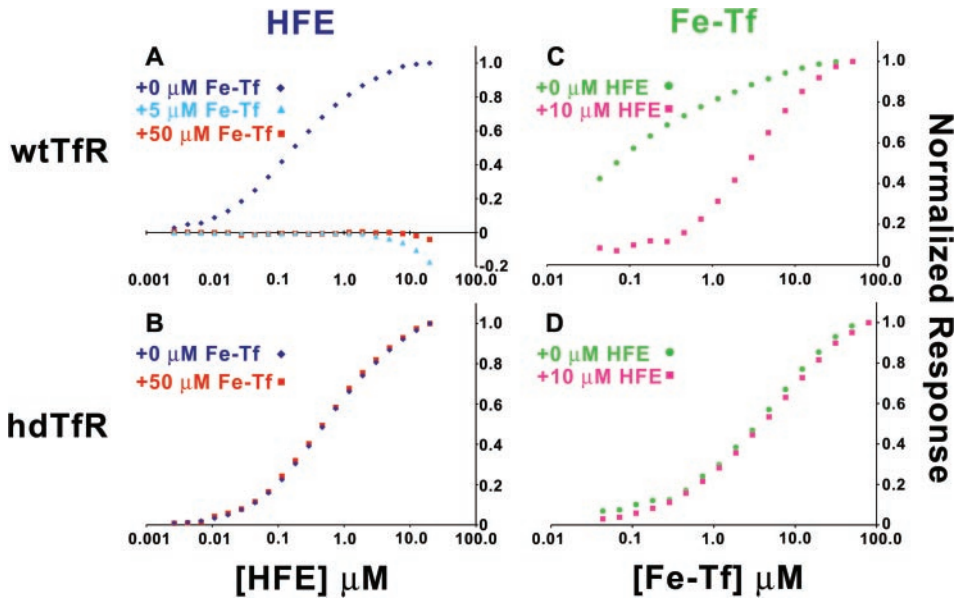

FIG. 5. **SPR assay of competition between HFE and Fe-Tf for binding to wtTfR *versus* hdTfR.** Plots are of the normalized equilibrium biosensor response value *versus* the log of the indicated protein concentration. HFE binding in the absence (*blue diamonds*) or presence of Fe-Tf (50 μM Fe-Tf (*red square*) and 5 μM Fe-T (*cyan triangle*)) to wtTfR (*A*) or to hdTfR (*B*). Fe-Tf binding is shown in the absence (*green circle*) or presence of 10 μM HFE (*magenta square*) to wtTfR (*C*) or to hdTfR (*D*). Data points are related by a 1.6-fold dilution series.

excess (50 μM) or near physiological (5 μM) (37) quantities of Fe-Tf (Fig. 5*A*), only a small amount of HFE binding was observed at the highest concentrations tested (Fig. 5*A*). This binding was observed as a decrease in SPR signal, because the binding of HFE requires the displacement of Fe-Tf, which is 1.8 times heavier than HFE, from its binding site on TfR (20, 24, 25). When Fe-Tf was injected in the presence of saturating amounts of HFE (10 μM), there was a reduction in Fe-Tf binding (Fig. 5*C*), consistent with previous reports that HFE reduces the observed binding affinity of Fe-Tf to TfR (8, 21, 23). Consistent with the lower TfR binding affinity of HFE as compared with Fe-Tf, HFE begins to compete with Fe-Tf for binding wtTfR only when it is present at a 4-fold or higher concentration than Fe-Tf, whereas Fe-Tf begins to compete with HFE for binding wtTfR when it is present at one-tenth the concentration of HFE. Taken together, these experiments confirm that HFE and Fe-Tf compete for TfR binding sites and rule out the effects of negative cooperativity in the HFE/hdTfR/Fe-Tf ternary interaction.

Cell Surface HFE Competes Effectively with Fe-Tf for Binding to Cell Surface TfR—The demonstration that negative cooperativity is not involved in heterotropic interactions between TfR, HFE, and Fe-Tf indicates that direct competition between HFE and Fe-Tf for binding to cell surface TfR is solely responsible for the observation that HFE lowers the affinity of TfR for Fe-Tf (5, 21, 23). Our SPR and AUC experiments demonstrate that soluble HFE competes poorly against Fe-Tf for TfR binding because of its lower affinity for TfR compared with Fe-Tf (Figs. 4*C* and 5*A*). Under physiological conditions, however, HFE and TfR are tethered to the same membrane (19), thereby increasing their effective local concentrations and permitting potential interactions between the HFE and TfR cytoplasmic tails (22). Either or both of these effects could allow HFE to compete more effectively against Fe-Tf for binding to TfR.

To evaluate how the addition of Fe-Tf affects complex formation between full-length HFE and TfR proteins tethered to a common membrane, we first showed that binding to TfR is required for a GFP-tagged form of HFE to traffic to Tf-positive endosomal compartments, and then asked if the addition of Fe-Tf affects endosomal localization of HFE-GFP. For these experiments, we expressed an HFE-GFP chimeric protein, in which GFP was fused to the C terminus of full-length HFE, in two forms of Chinese hamster ovary cells: TRVb cells, which lack expression of endogenous hamster TfR, and TRVb-1 cells, which lack endogenous TfR but stably express human TfR (36). Confocal imaging of HFE-GFP-expressing TRVb-1 (HFE^+/TfR^+) cells reveals primarily intracellular fluorescence (Fig. 6*A*, *middle panel*), which co-localizes with endocytosed Alexa-546-labeled human Fe-Tf (Fig. 6*A*, *right panel*), demonstrating that the HFE traffics to Tf-positive endosomes in cells expressing TfR. By contrast, most of the GFP fluorescence in HFE-GFP-expressing TRVb cells (HFE^+/TfR^-) was primarily localized at the cell surface (Fig. 6*A*, *left panel*), and these cells show no significant intracellular fluorescence in Alexa-546 Fe-Tf uptake experiments (data not shown). These data demonstrate that binding to cell surface TfR is required for HFE localization in Tf-positive endosomes, consistent with the lack of an obvious endocytic signal in the HFE cytoplasmic tail (3, 8, 21). Thus, endosomal localization of HFE-GFP can be used to evaluate competition between Fe-Tf and HFE for binding to cell surface TfR.

Since HFE binding to TfR is required for HFE translocation to Tf-positive endosomes, we investigated whether endosomal localization of HFE could be prevented by the presence of high concentrations of extracellular Fe-Tf. To address this question, we incubated TRVb-1-HFE-GFP (HFE^+/TfR^+) cells in growth medium supplemented with Fe-Tf at concentrations ranging from 0 nM to 50 μM. At relatively low concentrations of extracellular Fe-Tf (500 nM), HFE-GFP fluorescence began to redistribute from intracellular locations to the cell surface (Fig. 6*B*). Upon the addition of micromolar concentrations of Fe-Tf corresponding to serum Fe-Tf levels (37), we saw a substantial reduction of endosomal GFP fluorescence with a concomitant increase in cell surface fluorescence (Fig. 6*B*). At Fe-Tf concentrations exceeding 5 μM, little or no HFE-GFP fluorescence localized to endosomes, indicating that Fe-Tf has competed effectively with HFE to occupy virtually all binding sites on cell surface TfR molecules (Fig. 6*B*). The addition of the same concentrations of iron-loaded ovotransferrin, a transferrin ortholog that does not bind human TfR (38), did not result in detectable redistribution of HFE-GFP from endosomal compartments to the cell surface (Fig. 6*C*), indicating that the HFE

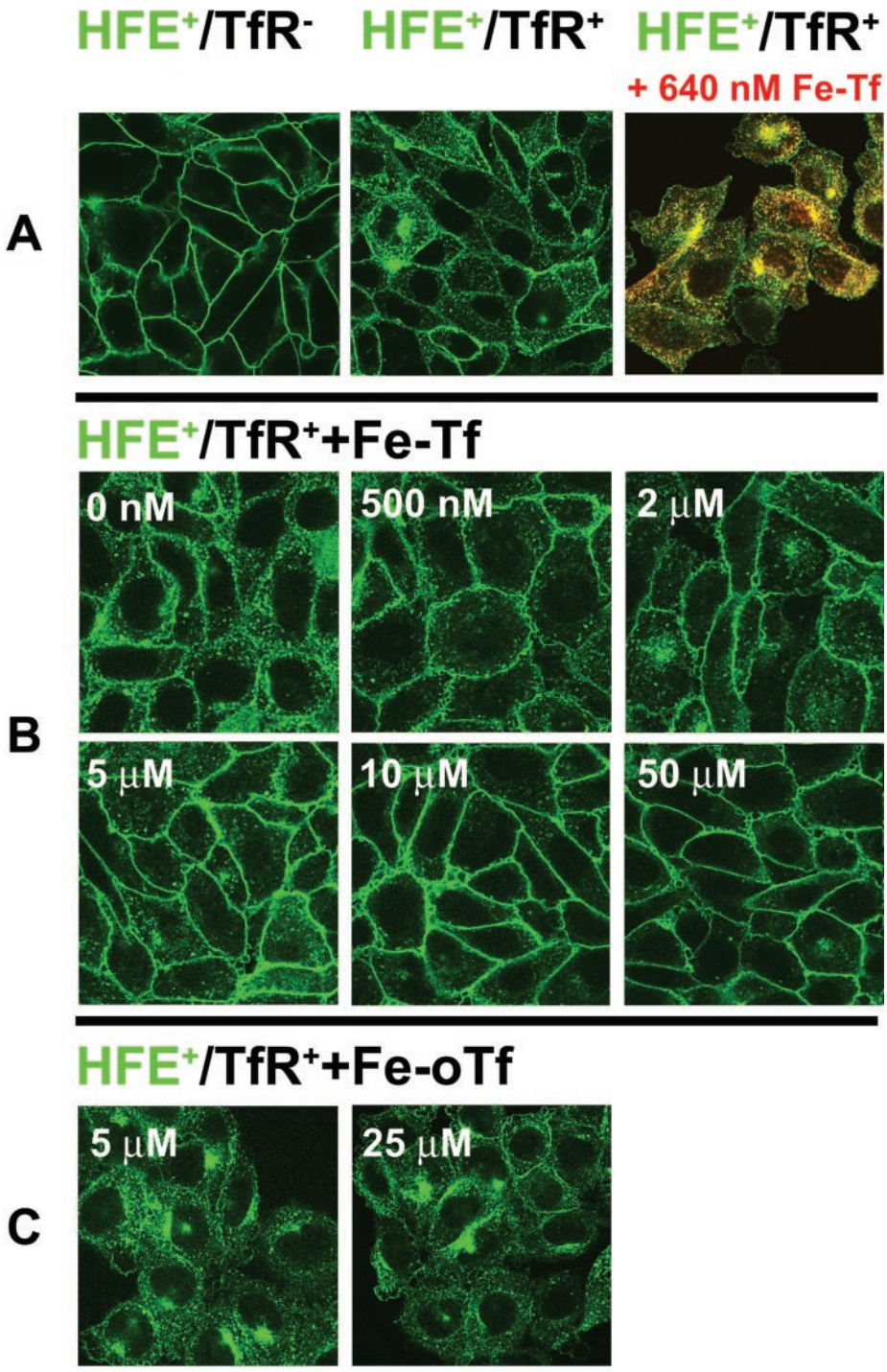

FIG. 6. **Confocal images of HFE-GFP distribution in TRVb (TfR$^-$) and TRVb-1 (TfR$^+$) cells.** *A*, cells expressing HFE-GFP (*green fluorescence*) in the absence (*left*) or presence (*middle*) of co-expressed human TfR. Co-localization of HFE-GFP fluorescence with Alexa-546-labeled human Fe-Tf in TfR$^+$ cells is shown on the *right*. *B*, cells expressing HFE-GFP and human TfR incubated with the indicated concentrations of unlabeled human Fe-Tf in the culture media. *C*, cells expressing HFE-GFP and TfR incubated with the indicated concentrations of chicken Fe-Tf (*Fe-oTf*) in the culture media.

redistribution effect is due to direct competition between HFE and human Fe-Tf for TfR binding sites.

DISCUSSION

TfR is a homodimeric receptor that binds two ligands at neutral or basic pH: Fe-Tf and HFE. TfR can form binary complexes with either HFE or Fe-Tf and can bind both ligands simultaneously to form a 1:1:1 HFE·TfR·Fe-Tf ternary complex (18–20). Characterizing the ternary complex is of interest, because both soluble and membrane-bound HFE reduce the apparent affinity of soluble and membrane-bound TfR for Fe-Tf (8, 21, 23, 39). Since mixtures of binary and ternary complexes form when all three proteins are present (Fig. 1), it has not been possible to determine if HFE reduces the affinity of TfR for Fe-Tf via direct competition for overlapping binding sites on TfR and/or if structural changes induced by HFE binding to one chain of the TfR dimer (19) lowers the binding affinity for ligand on the other TfR chain. Although several studies have demonstrated that HFE and Fe-Tf compete for binding to a common site on TfR (20, 24, 25), the potential role for negative cooperativity in the binding of Fe-Tf to 1:1 HFE·TfR complexes has not been addressed because of complications arising from the competing side reactions that lead to 2:1 HFE·TfR and Fe-Tf·TfR complexes when both HFE and Fe-Tf are incubated with homodimeric wtTfR. To directly evaluate the effects of heterotropic ligand binding to TfR, we constructed a hdTfR in which one chain binds HFE but not Fe-Tf and the other chain binds Fe-Tf but not HFE, such that only ternary complexes can form when hdTfR is incubated with Fe-Tf and HFE.

Although many substitutions in the TfR ligand-binding site affect binding to both ligands (20, 24), we were able to produce an hdTfR in which the HFE-binding chain retains a 390 nM affinity for HFE, but no detectable affinity for Fe-Tf, and the Fe-Tf-binding chain retains a 1.2 μM affinity for Fe-Tf but does not bind detectably to HFE (Fig. 3, *A–D*, Table I). Sedimentation velocity AUC and biosensor binding assays demonstrate that the hdTfR binds only one HFE and only one Fe-Tf and that it forms a 1:1:1 HFE·TfR·Fe-Tf ternary complex when all three proteins are mixed together. Having confirmed that hdTfR does not participate in side reactions leading to binary complexes (Fig. 1), we used it to evaluate whether binding of ligand to one chain of TfR affects the binding affinity of the other ligand for TfR. Biosensor binding assays conducted in the presence and absence of a saturating concentration of Fe-Tf reveal no significant differences in the binding affinity of HFE for hdTfR. Similarly, Fe-Tf binding to hdTfR is not altered by prebinding HFE to one chain of hdTfR. By contrast, when wtTfR is incubated with a saturating amount of HFE, we observe a reduction in the apparent binding affinity for Fe-Tf, as previously reported (23). The experiments using hdTfR demonstrate that there is no cooperativity, either negative or positive, in heterotropic ligand binding by hdTfR, suggesting that the apparent lowering of the Fe-Tf affinity of cell surface and soluble wtTfR by HFE (8, 23, 39, 40) results entirely from competition between HFE and Fe-Tf for overlapping binding sites on the TfR surface. Extending these results to wtTfR requires the assumption that the mutations used to create the hdTfR do not themselves disrupt cooperativity. Because we cannot evaluate cooperativity using wtTfR, we cannot directly address this issue. However, it is unlikely that the mutations themselves disrupt cooperativity, because the substituted residues are on the exterior of the protein in locations that are distant from the TfR dimer interface, across which structural changes would need to be propagated for cooperativity in ligand binding to occur.

Having shown that direct competition rather than allostery affects heterotropic ligand binding by TfR in solution, we next evaluated the effects of competition as a function of ligand concentration. Using wtTfR in a biosensor-based binding assay, we find that HFE shows only minimal binding to wtTfR when Fe-Tf is present at concentrations of 5 μM and above, demonstrating that it can compete with Fe-Tf, but only when it is several times more concentrated. Consistent with this result, sedimentation velocity AUC experiments show that 2:1 Fe-Tf·TfR complexes are the dominant species when HFE, Fe-Tf, and wtTfR are mixed such that the HFE and Fe-Tf are at higher concentrations than wtTfR. Therefore, soluble HFE is a poor competitor for binding to soluble TfR when Fe-Tf is present at high concentrations, including the micromolar concentrations corresponding to physiological levels of Fe-Tf in blood (37).

If TfR binding is required for HFE to act as a regulator of cellular iron homeostasis, then it must compete effectively against physiological levels of Fe-Tf when TfR and HFE are both present at the surface of a cell. Since HFE and TfR are tethered to the same cellular membrane (19), the effective concentrations of both proteins may be much higher than in the biochemical assays involving soluble proteins used here. We therefore developed a cell-based assay to evaluate the effects of the addition of soluble Fe-Tf on the interaction between membrane-bound HFE and membrane-bound TfR. As an indication of HFE·TfR complex formation, we monitored the localization of an HFE-GFP chimeric protein in transfected cells, assuming that HFE-GFP fluorescence in endosomes represents HFE-GFP that trafficked there as a result of binding to cell surface TfR. This assumption was verified by showing that HFE trafficks to Tf-positive endosomes in TfR-positive but not TfR-negative cells; thus, TfR binding is required for HFE to enter endosomes. By incubating the TfR-positive cells with Fe-Tf, we then demonstrated a loss of endosomal HFE-GFP fluorescence at relatively low concentrations of exogenous Fe-Tf (500 nM), with a substantial redistribution of GFP fluorescence to the cell surface at near physiological concentrations of exogenous Fe-Tf (micromolar) (37). Thus, external levels of Fe-Tf can influence both the localization and binding state of HFE in cells. The relatively high concentrations of Fe-Tf required to affect HFE localization and binding to TfR suggest a reevaluation of previous studies using transfected cells in which subphysiological concentrations of Fe-Tf were used as the iron source (7, 21, 22, 39–44). Our data suggest that redistribution of HFE at micromolar concentrations of Fe-Tf in blood has functional consequences that may not be observed in studies using submicromolar levels of Fe-Tf.

Indeed, competition between HFE and Fe-Tf for binding to TfR has been hypothesized to be critical for controlling iron metabolism (45, 46). In one model involving HFE/Fe-Tf competition, the concentration of Fe-Tf controls whether HFE binds to TfR, thereby inhibiting uptake of Fe-Tf, or if HFE binds to another cell surface protein (*e.g.* ferroportin, an iron-export protein (47–49)), thereby inhibiting export of intracellular iron. Although our results show that soluble HFE competes poorly with Fe-Tf for binding to soluble TfR, membrane-bound HFE can compete effectively with physiological concentrations of exogenous Fe-Tf for binding to cell surface TfR. Thus, the amount of cell surface HFE bound to cell surface TfR can be controlled by the concentration of exogenous Fe-Tf, alone or in concert with changes in TfR expression levels, allowing regulation of the binding configuration of HFE at the cell surface. There are three possible binding configurations of HFE at the cell surface (bound to TfR, bound to another protein(s), or free), each of which could be involved in regulation of iron homeostasis. For example, HFE bound to TfR can prevent uptake of iron in the form of Fe-Tf. If Fe-Tf binding to TfR competes away HFE, allowing it to bind to an iron transport protein such as ferroportin or DMT1 (an iron import protein (50)), then fluctuations in the level of free *versus* bound HFE could regulate either the rate of cellular iron export (ferroportin) or import (DMT1). Additionally, if cells can sense the amount of cell surface or endosomally localized HFE, then fluctuations in those levels could affect downstream signaling.

Elucidating the details of the interactions between HFE, TfR, and Fe-Tf will be critical for understanding the mechanisms by which mammals regulate iron levels. We have clarified the interactions between these proteins, demonstrating that several TfR/ligand stoichiometries are possible, that HFE/TfR binding is required for HFE transport to endosomes, and that there is strong allostery-free competition between HFE and Fe-Tf for TfR binding at the cell surface. These results provide experimental support for models of iron regulation in which competition between HFE and Fe-Tf for binding to TfR plays a central role in maintaining cellular iron homeostasis (45).

Acknowledgments—We thank Peter Snow, Inderjit Nangiana, and Cynthia Jones (Caltech Protein Expression Facility) for insect cell expression of TfR constructs; Tim McGraw (Cornell) for providing TRVb and TRVb-1 cells; W. Lance Martin and Jasvinder Nangiana for construction of expression vectors; Rochelle Diamond (Caltech Cell Sorting Facility) for cell sorting; Kirsten Lassila for assistance with CD data collection; the Beckman Imaging Center at Caltech for providing confocal microscopes and support; Andrew Herr, Caroline Enns, Devin Tesar, and Rich Olson for helpful discussions; Dave Myszka for beta versions of Scrubber and Clamp; and members of the Björkman laboratory for critical reading of the manuscript.

REFERENCES

1. Cullen, L. M., Anderson, G. J., Ramm, G. A., Jazwinska, E. C., and Powell, L. W. (1999) *Annu. Rev. Med.* **50,** 87–98
2. Bothwell, T. H., and MacPhail, A. P. (1998) *Semin. Hematol.* **35,** 55–71
3. Feder, J. N., Gnirke, A., Thomas, W., Zsuchihashi, Z., Ruddy, D. A., Basava, A., Dormishian, F., Domingo, R., Ellis, M. C., Fullan, A., Hinton, L. M., Jones, N. L., Kimmel, B. E., Kronmal, G. S., Lauer, P., Lee, V. K., Loeb, D. B., Mapa, F. A., McCellland, E., Meyer, N. C., Mintier, G. A., Moeller, N., Moore, T., Morikang, E., Prass, C. E., Quintana, L., Starnes, S. M., Schatzman, R. C., Brunke, K. J., Drayna, D. T., Risch, N. J., Bacon, B. R., and Wolff, R. K. (1996) *Nat. Genet.* **13,** 399–408
4. Garcia, K. C., Teyton, L., and Wilson, I. A. (1999) *Annu. Rev. Immunol.* **17,** 369–397
5. Feder, J. N., Tsuchihashi, Z., Irrinki, A., Lee, V. K., Mapa, F. A., Morikang, E., Prass, C. E., Starnes, S. M., Wolff, R. K., Parkkila, S., Sly, W. S., and Schatzman, R. C. (1997) *J. Biol. Chem.* **272,** 14025–14028
6. Waheed, A., Parkkila, S., Zhou, X. Y., Tomatsu, S., Tsuchihashi, Z., Feder, J. N., Schatzman, R. C., Britton, R. S., Bacon, B. R., and Sly, W. S. (1997) *Proc. Natl. Acad. Sci. U. S. A.* **94,** 12384–12389
7. Roy, C. N., Carlson, E. J., Anderson, E. L., Basava, A., Starnes, S. M., Feder, J. N., and Enns, C. A. (2000) *FEBS Lett.* **484,** 271–274
8. Feder, J. N., Penny, D. M., Irrinki, A., Lee, V. K., Lebrón, J. A., Watson, N., Tsuchihashi, Z., Sigal, E., Bjorkman, P. J., and Schatzman, R. C. (1998) *Proc. Natl. Acad. Sci. U. S. A.* **95,** 1472–1477
9. Parkkila, S., Waheed, A., Britton, R. S., Bacon, B. R., Zhou, X. Y., Tomatsu, S., Fleming, R. E., and Sly, W. S. (1997) *Proc. Natl. Acad. Sci. U. S. A.* **94,** 13198–13202
10. Leibman, A., and Aisen, P. (1977) *Biochemistry* **16,** 1268–1272
11. Rothenberger, S., Iacopetta, B. J., and Kuhn, L. C. (1987) *Cell* **49,** 423–431
12. Collawn, J. F., Kuhn, L. A., Liu, L. F., Tainer, J. A., and Trowbridge, I. S. (1991) *EMBO J.* **10,** 3247–3253
13. Collawn, J. F., Lai, A., Domingo, D., Fitch, M., Hatton, S., and Trowbridge, I. S. (1993) *J. Biol. Chem.* **268,** 21686–21692
14. Sipe, D. M., and Murphy, R. F. (1991) *J. Biol. Chem.* **266,** 8002–8007
15. Bali, P. K., Zak, O., and Aisen, P. (1991) *Biochemistry* **30,** 324–328
16. Dautry-Varsat, A., Ciechanover, A., and Lodish, H. F. (1983) *Proc. Natl. Acad. Sci. U. S. A.* **80,** 2258–2262
17. Enns, C. A., and Sussman, H. H. (1981) *J. Biol. Chem.* **256,** 9820–9823
18. Lebrón, J. A., Bennett, M. J., Vaughn, D. E., Chirino, A. J., Snow, P. M., Mintier, G. A., Feder, J. N., and Bjorkman, P. J. (1998) *Cell* **93,** 111–123
19. Bennett, M. J., Lebrón, J. A., and Bjorkman, P. J. (2000) *Nature* **403,** 46–53
20. West, A. P., Jr., Giannetti, A. M., Herr, A. B., Bennett, M. J., Nangiana, J. S., Pierce, J. R., Weiner, L. P., Snow, P. M., and Bjorkman, P. J. (2001) *J. Mol. Biol.* **313,** 385–397
21. Gross, C. N., Irrinki, A., Feder, J. N., and Enns, C. A. (1998) *J. Biol. Chem.* **273,** 22068–22074
22. Salter-Cid, L., Brunmark, A., Li, Y., Leturcq, D., Peterson, P. A., Jackson, M. R., and Yang, Y. (1999) *Proc. Natl. Acad. Sci. U. S. A.* **96,** 5434–5439
23. Lebrón, J. A., West, A. P., and Bjorkman, P. J. (1999) *J. Mol. Biol.* **294,** 239–245
24. Giannetti, A. M., Snow, P. M., Zak, O., and Bjorkman, P. J. (2003) *PLoS. Biol.* **1,** 341–350
25. Liu, R., Guan, J. Q., Zak, O., Aisen, P., and Chance, M. R. (2003) *Biochemistry* **42,** 12447–12454
26. Cheng, Y., Zak, O., Aisen, P., Harrison, S. C., and Walz, T. (2004) *Cell* **116,** 565–576
27. Lawrence, C. M., Ray, S., Babyonyshev, M., Galluser, R., Borhani, D. W., and Harrison, S. C. (1999) *Science* **286,** 779–782
28. Lebrón, J. A., and Bjorkman, P. J. (1999) *J. Mol. Biol.* **289,** 1109–1118
29. Schmidt, T. G., Koepke, J., Frank, R., and Skerra, A. (1996) *J. Mol. Biol.* **255,** 753–766
30. Voss, S., and Skerra, A. (1997) *Protein Eng.* **10,** 975–982
31. Fägerstam, L. G., Frostell-Karlsson, A., Karlsson, R., Persson, B., and Rönnber, I. (1992) *J. Chromatogr.* **597,** 397–410
32. Malmqvist, M. (1993) *Nature* **361,** 186–187
33. Morton, T. A., and Myszka, D. G. (1998) *Methods Enzymol.* **295,** 268–294
34. Schuck, P. (2000) *Biophys. J.* **78,** 1606–1619
35. Brewer, C. B., and Roth, M. G. (1991) *J. Cell Biol.* **114,** 413–421
36. McGraw, T. E., Greenfield, L., and Maxfield, F. R. (1987) *J. Cell Biol.* **105,** 207–214
37. Henry, J. B. (1991) *Clinical Diagnosis and Management by Laboratory Methods*, W. B. Saunders Co., Philadelphia
38. Shimo-Oka, T., Hagiwara, Y., and Ozawa, E. (1986) *J. Cell. Physiol.* **126,** 341–351
39. Roy, C. N., Penny, D. M., Feder, J. N., and Enns, C. A. (1999) *J. Biol. Chem.* **274,** 9022–9028
40. Riedel, H. D., Muckenthaler, M. U., Gehrke, S. G., Mohr, I., Brennan, K., Herrmann, T., Fitscher, B. A., Hentze, M. W., and Stremmel, W. (1999) *Blood* **94,** 3915–3921
41. Corsi, B., Levi, S., Cozzi, A., Corti, A., Altimare, D., Albertini, A., and Arosio, P. (1999) *FEBS Lett.* **460,** 149–152
42. Feeney, G. P., and Worwood, M. (2001) *Biochim. Biophys. Acta* **1538,** 242–251
43. Waheed, A., Grubb, J. H., Zhou, X. Y., Tomatsu, S., Fleming, R. E., Costaldi, M. E., Britton, R. S., Bacon, B. R., and Sly, W. S. (2002) *Proc. Natl. Acad. Sci. U. S. A.* **99,** 3117–3122
44. Montosi, G., Paglia, P., Garuti, C., Guzman, C. A., Bastin, J. M., Colombo, M. P., and Pietrangelo, A. (2000) *Blood* **96,** 1125–1129
45. Townsend, A., and Drakesmith, H. (2002) *Lancet* **359,** 786–790
46. Drakesmith, H., Sweetland, E., Schimanski, L., Edwards, J., Cowley, D., Ashraf, M., Bastin, J., and Townsend, A. R. (2002) *Proc. Natl. Acad. Sci. U. S. A.* **99,** 15602–15607
47. McKie, A. T., Marciani, P., Rolfs, A., Brennan, K., Wehr, K., Barrow, D., Miret, S., Bomford, A., Peters, T. J., Farzaneh, F., Hediger, M. A., Hentze, M. W., and Simpson, R. J. (2000) *Mol. Cell* **5,** 299–309
48. Donovan, A., Brownlie, A., Zhou, Y., Shepard, J., Pratt, S. J., Moynihan, J., Paw, B. H., Drejer, A., Barut, B., Zapata, A., Law, T. C., Brugnara, C., Lux, S. E., Pinkus, G. S., Pinkus, J. L., Kingsley, P. D., Palis, J., Fleming, M. D., Andrews, N. C., and Zon, L. I. (2000) *Nature* **403,** 776–781
49. Abboud, S., and Haile, D. J. (2000) *J. Biol. Chem.* **275,** 19906–19912
50. Gunshin, H., Mackenzie, B., Berger, U. V., Gunshin, Y., Romero, M. F., Boron, W. F., Nussberger, S., Gollan, J. L., and Hediger, M. A. (1997) *Nature* **388,** 482–488